Control of an Aircraft Electric Fuel Pump Drive

JIMMIE J. CATHEY
University of Kentucky
JOSEPH A. WEIMER
Aero Propulsion Laboratory

The concept of designing a high-speed, permanent magnet, brushless dc motor aircraft fuel pump drive using a cycloconverter link is examined. A closed-loop control system with an outer loop on speed and an inner loop on current is postulated wherein a proportional plus integral controller is placed in the forward path to assure minimum speed error. Gains are then set to assure that the eigenvalues of the linearized control system lie within the left half *s*-plane over full speed range.

Manuscript received June 25, 1987.

This work was supported by the Aero Propulsion Laboratory, Air Force Wright Aeronautical Laboratories under Contract F33615-81-C-201, Subcontract SCEE/SRAP/84-17A.

Authors' addresses: Cathey, Dep't. of Electrical Engineering, University of Kentucky, Lexington, KY 40506; Weimer, Aero Propulsion Laboratory, Wright-Patterson Air Force Base, OH 45433.

I. INTRODUCTION

Losses associated with pumping fuel over a relief valve in an aircraft can be eliminated by utilizing a pump drive with speed independent of engine speed. Further, an electric fuel pump drive lends itself to ease of interface with any intelligent control regime of the aircraft engine.

The brushless dc motor is a desireable candidate for an electric pump drive due to the potential for design that combines ruggedness and high reliability with a small volume. In particular, a cycloconverter link drive is of interest over a dc link drive since it uses no bulky filter capacitor, controls simply for reverse power flow to quickly reduce pump speed, offers commutation advantage in that voltage potential at the anode of a commutating silicon controlled rectifier (SCR) inherently decreases, and requires no alternative control strategy for start-up or low speed operation.

Many publications relating to the brushless dc drive are available. Several works have appeared dealing with open-loop cycloconverter driven brushless dc motor performance [1–6]. Also, of pertinence to this study are three papers that deal with closed-loop speed control of the dc link brushless dc drive [7–9]. However, the literature does not seem to contain an analysis of the cycloconverter link phase modulation (PM) brushless dc drive under closed-loop speed control.

II. ANALYSIS APPROACH

A power circuitry schematic of the midpoint cycloconverter drive is shown in Fig. 1. Present analysis is concerned with the control of average developed torque and power flow rather than instantaneous quantities. Advantage is taken of this particular concern to develop steady-state descriptions that are considerably simplified over those necessary to account for energy conversion occurring at harmonic frequencies.

Combinations of sinusoidal steady-state and dc steady-state analysis are utilized to obtain a suitable model of the motor. The effective magnetomotive force (MMF) angle (γ) is then examined as phase current magnitude is varied to determine a control strategy for the no-load MMF angle (γ_0) to assure successful SCR commutation. A closed-loop control system is then postulated. Since the equations describing the motor developed torque and generated electromotive force (EMF) are nonlinear, the resulting control system equations are nonlinear. A small perturbation model is derived allowing gain adjustment to assure stability and to adjust transient response. Dynamic equations of the system, based on average value of motor phase current, are then formulated and numerically solved to study transient performance.

III. STEADY-STATE MOTOR DESCRIPTION

Assuming that the motor is designed such that airgap flux density due to phase modulation (PM) poles is

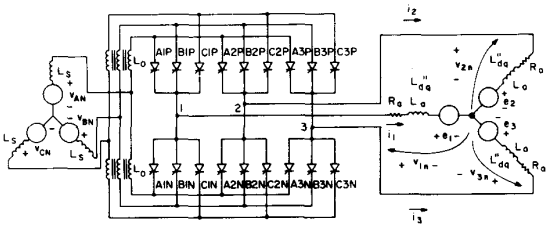

Fig. 1. Schematic of cycloconverter drive power circuitry.

sinusoidal with respect to the rotor, then as the rotor revolves, the generated counter EMF per phase will vary sinusoidally with respect to time. Fig. 2(a) establishes the relationship between the fundamental component (i_{11}) of motor phase current (i_1), phase counter EMF (e_1), and the PM field supported MMF ($\mathcal{F}_F$). Neglecting commutation overlap, only two stator windings conduct current at any instant in time. The space phasor diagram of Fig. 2(b) shows the average position armature reaction MMF ($\mathcal{F}_{ar}$) with respect to $\mathcal{F}_F$ for a 60° interval during

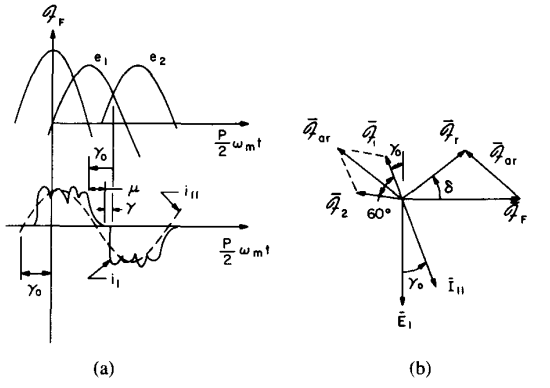

(a) (b)

Fig. 2. Angular relationships between electrical and magnetic quantities. (a) Time diagram. (b) Phasor diagram.

which phases 1 and 2 are conducting current. Projection of $\mathcal{F}_r$ and $\mathcal{F}_{ar}$ on the horizontal allows us to write the following relationship involving torque angle (δ):

$$\tan\delta = \frac{\mathcal{F}_{ar}\cos(\delta_0 + 30°)}{\mathcal{F}_F - \mathcal{F}_{ar}\sin(\gamma_0 + 30°)} \cdot \tag{1}$$

Letting I_{AC} be the average value of i_1 over a conduction interval, p be the number of poles, and L_m be the synchronous inductance, then (1) can be solved for the torque angle as

$$\delta = \tan^{-1}\left[\frac{\sqrt{2}\,p\,L_m I_{AC}\cos(\gamma_0 + 30°)}{\pi K_m - \sqrt{2}\,p\,L_m I_{AC}\sin(\gamma_0 + 30°)}\right] \cdot \tag{2}$$

In order to find an expression for the commutation overlap angle (μ), we must examine the circuit of Fig. 1 (over the interval μ) wherein i_1 is decaying and i_2 is rising so that both SCR 1P and 2P are conducting. Since during this interval terrminals 1 and 2 of the motor are effectively shorted, KVL requires that

$$e_1 + L''_{dq}\frac{di_1}{dt} \equiv e_2 + L''_{dq}\frac{di_2}{dt} \cdot \tag{3}$$

Equation (3) can be multiplied by dt, integrated over the interval μ, and solved for μ to yield

$$\mu = \gamma_0 - \cos^{-1}\left[\frac{\sqrt{3}\,pL''_{dq}I_{AC}}{K_m} + \cos\gamma_0\right] \tag{4}$$

where $I_{AC} \simeq \frac{1}{2}\,[i_1(0) + i_2(\mu/\omega)]$.

A per phase equivalent circuit can now be drawn for the motor as displayed by Fig. 3(a) where the associated phasor diagram of Fig. 3(b) properly accounts for the

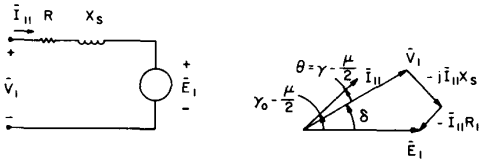

(a) (b)

Fig. 3. Per phase model. (a) Equivalent circuit. (b) Phasor diagram.

effective phase shift ($\mu/2$) of phase current due to commutation overlap. Total developed torque can now be found by calculating the total power delivered to E_1 and dividing by motor mechanical speed (μ_m). The result is

$$T_d = \frac{3\sqrt{3}}{\pi}K_m I_{AC}\cos\left(\gamma_0 - \frac{\mu}{2}\right) \cdot \tag{5}$$

In order to complete the motor model, a method to calculate the conduction interval average value of phase current i_1 remains. The procedure to be used is that of finding a dc steady-state model valid over a 60° step of the motor period. Due to symmetry of the problem, if a valid model can be established for any 60° step, then it is applicable to the following step, ad infinitum.

Looking back from the ideal cycloconverter output terminals back to the source during any 60° step, one sees a three-pulse phase-controlled converter which can be modelled by a series-connected dc source (V_d) and resistor as shown in Fig. 4. The average value of rectified voltage for an ideal half-wave three-phase source is V_d. The variable R_d models the resistance of the source and the chokes plus accounts for the effective voltage drop associated with the commutation notch due to source and choke coil inductance. Viewing the motor from the input terminals of the ideal cycloconverter during the same 60° step, it also appears as a three-pulse phase-controlled converter that can be modelled by a series combination of an average dc source (E_{eq}) and resistor as also shown in Fig. 4. However, in this latter case, it is convenient to model the dc source (E_{eq}) so that the voltage drop due to the commutation overlap is accounted for directly in calculation of E_{eq} [6], thus,

$$E_{eq} = \frac{3\sqrt{3}}{2\pi}K_m\,\omega_m\cos\left(\frac{\mu}{2}\right)\cos\left(\gamma_0 - \frac{\mu}{2} - \delta\right) \cdot \tag{6}$$

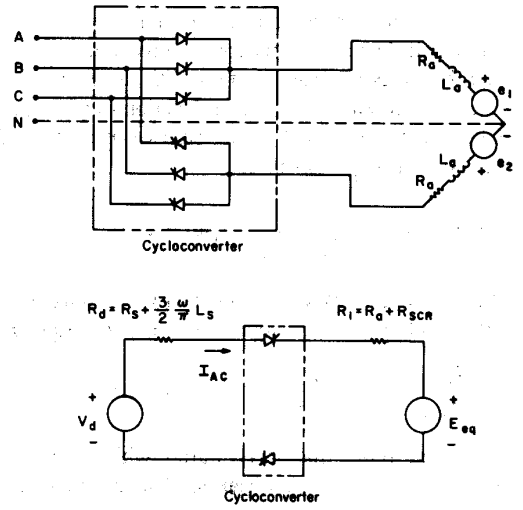

Fig. 4. Equivalent circuit for 60° interval.

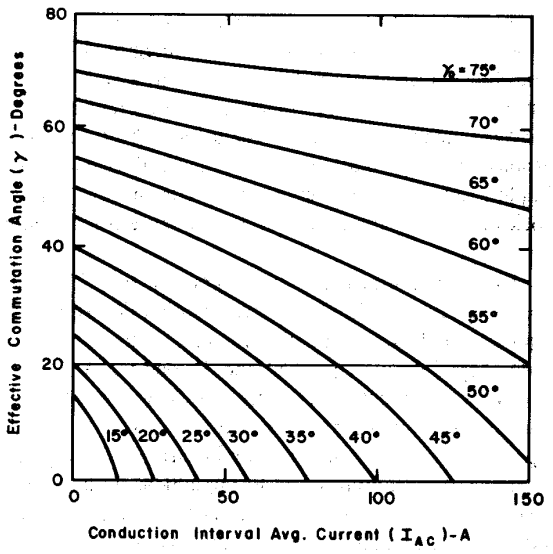

Fig. 5. Effective commutation angle (γ).

Application of KVL to the circuit of Fig. 4 leads to an expression for I_{AC}.

$$I_{AC} = \frac{\frac{3\sqrt{3}}{2\pi}\left[\sqrt{2}\,V\cos\alpha_s - K_m\omega_m\cos\left(\frac{\mu}{2}\right)\cos\left(\gamma_0 - \frac{\mu}{2} - \delta\right)\right]}{R_1 + R_s + \frac{3}{2}\frac{\omega}{\pi}L_s}. \quad (7)$$

Tsuchiya [6] has illustrated that the effective angle (γ) available for commutation of an SCR is

$$\gamma = \gamma_0 - \mu - \delta. \quad (8)$$

Both μ and δ increase with an increase in the magnitude of phase current as can be seen by inspection of (2) and (4). A large fixed value of γ_0 can be set by the control system, but leads to a reduced power factor and increase in harmonic torque at light load. A regime must necessarily be established to control γ_0 as a function of phase current magnitude. In order to see the nature of MMF angle control required, a family of curves is calculated and graphed in Fig. 5 to show commutation angle γ as a function of I_{AC} with γ_0 as a parameter. Arbitrarily selecting an effective commutation angle (γ) of 20° as acceptable (indicated by horizontal line of Fig. 5), information is now available to determine a value of γ_0 for each value of phase current. A plot of the resulting γ_0 versus I_{AC} is given by Fig. 6.

Since introduction of further nonlinearity into the system equations is undesirable, a relationship for γ_0 is selected as follows:

$$\gamma_0 = \gamma_0' + K_{\gamma I}\, I_{AC} + K_{\gamma\omega}\,\omega_m \quad (9)$$

where an ω_m dependent term is introduced to allow adequate recovery time for commutated SCRs at high motor speed operation. In accordance with (9), a straight line fit to the curve of Fig. 6 is made as indicated by the solid line to set values for γ_0' and $K_{\gamma I}$. For final implementation, the straight line approximation of γ_0 was

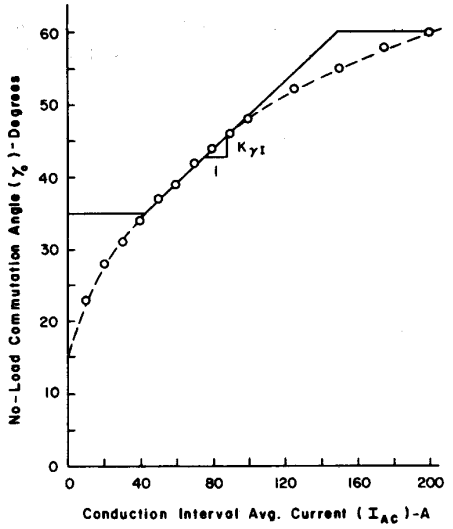

Fig. 6. γ_0 to maintain γ = 20°.

abandoned on the two extremes of I_{AC}. First, a value of γ_0 greater than 60° results in a poor power factor, thus γ_0 was limited to no more than 60°. Second, the later mentioned eigenvalue study showed that stability was enhanced if γ_0 was limited to no less than 35°.

IV. CONTROL SYSTEM DEVELOPMENT

In the fuel pump, application flow rate is related to speed. Thus motor speed is to be the controlled variable,

and a system is postulated wherein an outer loop is formed on speed. A proportional-plus-integral (PI) controller is placed in the forward path to assure minimum speed error. An inner loop on current is introduced since such usually enhances stability in fast response power conditioning drives as well as provides a simple mechanism for implementing current limit. A block diagram of the proposed control system is given by Fig. 7.

An inspection of the block diagram of Fig. 7 shows three areas for which a nonlinear equation description is required: 1) electrical equation relating V_d to I_{AC}, 2) developed torque equation, and 3) load torque expressed as a function of motor speed. The feedback gain changes implied by a break in the I_F versus I_{AC} and Ω_m versus ω_m curves are also nonlinearities. However, the transitions are introduced to implement limit at values greater than those of normal steady-state operating range, and thus, are ignored in steady-state analysis work.

Performance analysis of the system as interrelated by the block diagram of Fig. 7 is possible by numerical methods; however, any stability or compensation study becomes largely a trial and error process. The commonly used approach when confronted with a nonlinear system of equations is to linearize the equations about an operating point, and then to study stability and apply compensation to these small perturbation equations.

For the linearization process, the following variables are to be represented as a quiescent value plus a small variation where the quiescent values satisfy the original nonlinear equation at a particular operating point:

$$E_{eq} = E_0 + e \tag{10}$$

$$I_{AC} = I_0 + i \tag{11}$$

$$\Omega_m = \Omega + \omega \tag{12}$$

$$T_d = T_{d0} + \tau_d \tag{13}$$

$$T_L = T_{L0} + \tau_L. \tag{14}$$

Referring to (7), the term $V \cos \alpha_s$ $(= V_d)$ can be replaced by

$$V_d = A\, V_c \tag{15}$$

if cosine crossing firing angle control hardware is implemented; thus no nonlinearity is involved. Equation (7) then becomes a linear equation if E_{eq} as expressed by (6) can be represented as a linear function of speed and current. Using a truncated Taylor series expansion of E_{eq}, the variation in E_{eq} is given as

$$e = \left.\frac{\partial E_{eq}}{\partial \Omega_m}\right|_0 \omega + \left.\frac{\partial E_{eq}}{\partial I_{AC}}\right|_0 i = A_1 \omega + B_1 i. \tag{16}$$

The developer torque as given by (5) is similarly linearized yielding the variation in developed torque as

$$\tau_d = \left.\frac{\partial T_d}{\partial \Omega_m}\right|_0 \omega + \left.\frac{\partial T_d}{\partial I_{AC}}\right|_0 i = C_1 \omega + D_1 i. \tag{17}$$

For a load torque that varies purely with the nth power of motor speed, the variation of load torque is given by

$$\tau_L = \left.\frac{\partial T_L}{\partial \Omega_m}\right|_0 \omega = \frac{n\, k_T\, \Omega_m^{n-1}}{H_\omega^n} = T_1\, \omega. \tag{18}$$

Based on the above work, a block diagram of the small perturbation control system can be drawn as in Fig. 8. Application of Mason's gain formula to the block diagram of Fig. 8 leads to the characteristic equation of the small perturbation model as

$$\begin{aligned}\Delta_C = {} & \tau_\omega J[B_1 + R_{eq} + K_I A\, H_I]s^2 \\ & + \tau_\omega[(B_1 + R_{eq} + K_I A\, H_I)(\beta - C_1 + T_1) \\ & + A_1 D_1 + H_\omega K_\omega\, K_I D_I\, A]s \\ & + [H_\omega K_\omega K_I D_1\, A] = 0.\end{aligned} \tag{19}$$

Second-order equation (19) can be examined for system stability and gain constants adjusted to give desired response at any operating point. Trial and error work using a computer program to iteratively solve for the steady-state operating point values, to generate quiescent point constants, and to evaluate the characteristic equation roots (eigenvalues) shows that the system stability is quite sensitive to the value of current feedback gain (H_I) [10]. A set of system gains has been

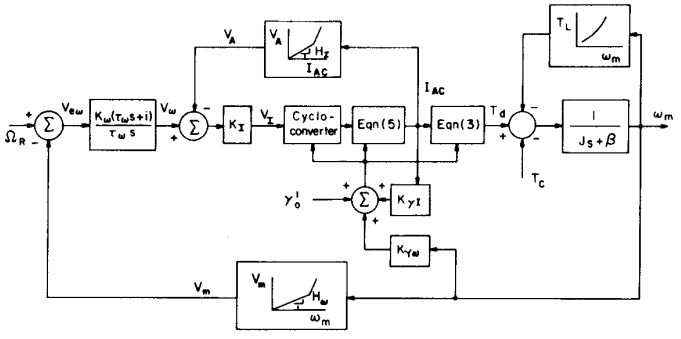

Fig. 7. Closed-loop control system.

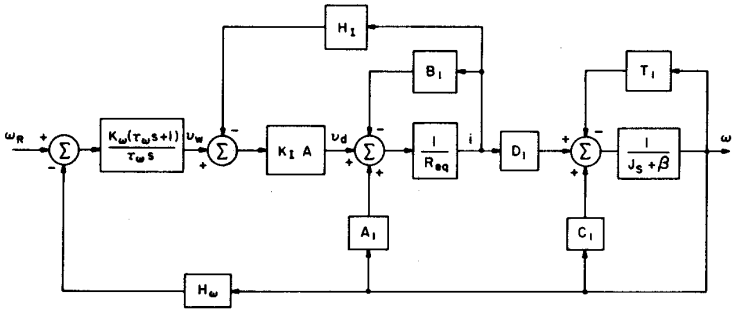

Fig. 8. Block diagram of linearized control system.

determined to assure stability across the motor speed range from 0 to 45,000 while resulting in a transient response of sufficient duration to be acceptable. The gains used for this study are listed in Table I.

TABLE I
Control System Gains

Gain	Value
H_I	0.05
H_ω	0.002122
K_I	5.80
K_ω	50.0
τ_ω	0.50
$K_{\gamma I}$	0.23333
$K_{\gamma\omega}$	0.002122

V. TRANSIENT MODEL FORMULATION

From the block diagram of Fig. 7, the set of differential equations that describes the system behavior using average value of current can be written as

$$\frac{d\omega_m}{dt} = \frac{1}{J}\left[\frac{3\sqrt{3}}{\pi} K_m I_{AC} \cos\left(\gamma_0 - \frac{\mu}{2}\right) - \beta\omega_m - k_T\,\omega_m^2\right] \tag{20}$$

$$\frac{dV_\omega}{dt} = \frac{K_\omega}{\tau_\omega}(\Omega_R - H_\omega\omega_m) + K_\omega\left(\frac{d}{dt}\Omega_R - H_\omega\frac{d\omega_m}{dt}\right) \tag{21}$$

where

$$I_{AC} = \frac{AK_I V_\omega - \frac{3}{2}\frac{\sqrt{3}}{\pi} K_m\omega_m \cos\left(\frac{\mu}{2}\right)\cos\left(\gamma_0 - \frac{\mu}{2} - \delta\right)}{R_1 + R_s + \frac{3}{2}\frac{\omega}{\pi}L_s + A\,K_I\,H_I} \tag{22}$$

and δ, μ, and γ_0 are given by (2), (4), and (9), respectively.

The above equation set offers tremendous computational advantages over the set necessary if instantaneous currents are used. First, the set contains two differential equations rather than five. Second, having removed the instantaneous currents, the remaining dependent differential equation variables vary more slowly with time allowing a solution interval several orders of magnitude greater than is necessary for the equations using instantaneous current.

VI. PERFORMANCE CALCULATIONS

The studies reported use a three-phase source of 400 Hz with 183.6 V line-to-neutral. However, the model is general so that any additional source frequency and voltage conditions can be examined by simple input data change. Load torque is assumed to vary with speed squared. Table II documents the parameters of the four-pole motor and pump examined.

TABLE II
Motor And Pump Parameters

Parameter	Symbol	Value
Winding resistance (phase, 180°C)	R_a	0.0127 Ω
Commutating inductance (phase)	L''_{dq}	0.015 mH
Synchronous inductance (phase)	L_m	0.030 mH
EMF constant	K_m	0.039057 V·s/rad
Inertia (total)	J	0.0017266 kg·m²
Damping coefficient (total)	β	9.72×10^{-5} N·m·s/rad
Load torque constant	k_T	3.2×10^{-7} N·m·s²/rad²

Although numerous conditions were studied, two representative cases are presented: 1) speed runup from 4500 to 45,000 rpm (Fig. 9), and 2) speed rundown from 45,000 to 24,000 rpm (Fig. 10).

VII. CONCLUSIONS

The brushless dc motor driven from a cycloconverter link is exactly described by a sequence of nonlinear circuit transients that are boundary interfaced. Performance solutions are tedious even for the steady-state case. This work has used a combination of sinusoidal and dc steady-state analysis to produce a simple model.

Although the work is not presented herein, results have been compared against the "exact system" in which

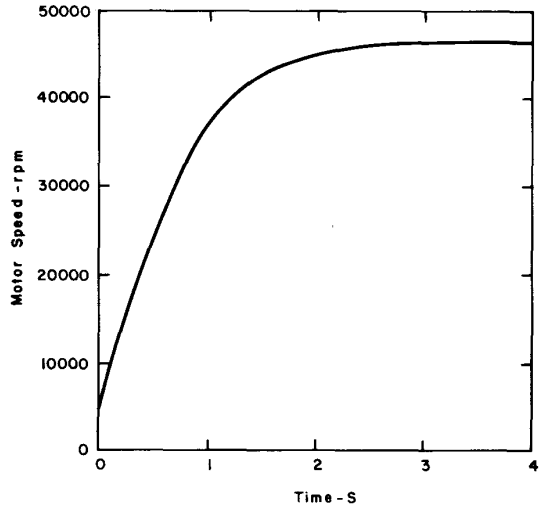

Fig. 9. 4,500 to 45,000 rpm speed runup.

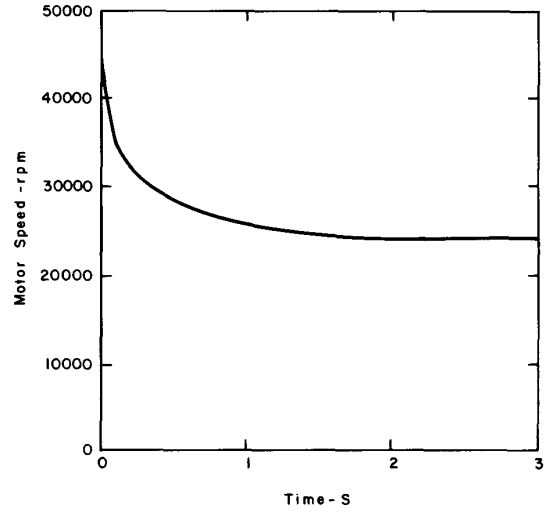

Fig. 10. 45,000 to 24,000 rpm speed rundown.

differential equation set was augmented to contain the instantaneous motor phase currents; the simple model of this paper was found to yield speed and current results that differ negligibly from the "exact" solution except for small currents at high speed where the neglected commutation overlap is no longer negligible.

The great advantage of this simplified model lies in the computational efficiency gained by a reduction in the number of differential equations and by allowing a solution interval for the differential equations that is four orders of magnitude greater than that required by the "exact" model.

REFERENCES

[1] Bourbeau, F.J. (1977)
Synchronous motor railcar propulsion.
IEEE Transactions on Industry Applications, IA-13, 1 (Jan./Feb. 1977), 8–17.

[2] Cornell, E.P., and Novotny, D.W. (1973)
Theoretical analysis of the stability and transient response of self-controlled synchronous machines.
Presented at the IEEE Power Electronics Specialists Winter Meeting, Jan. 1973, Paper C73144-3.

[3] Sato, N. (1964)
A study of the commutatorless motor.
Electrical Engineering of Japan, 84 (Aug. 1964), 45–52.

[4] Maeno, T., and Kobata, M. (1972)
AC commutatorless and brushless motor.
IEEE Transactions on Power Apparatus and Systems, PAS-91, 4 (July/Aug. 1972), 1476–1484.

[5] Cornell, E.P., and Novotny, D.W. (1974)
Commutation by armature induced voltage in self-controlled synchronous machines.
IEEE Transactions on Power Apparatus and Systems, PAS-93 (1974), 760–766.

[6] Tsuchiya, T. (1970)
Basic characteristics of cycloconverter-type commutatorless motors.
IEEE Transactions on Industry and General Applications, IGA-6, 4 (July/Aug. 1970), 349–356.

[7] Kataoka, T., and Nishikata, S. (1978)
Transient analysis of dc commutatorless motor.
Electrical Engineering of Japan, 98, 3 (1978), 82–89.

[8] Kataoka, T., and Nishikata, S. (1981)
Transient performance analysis of self-controlled synchronous motors.
IEEE Transactions on Industry Applications, IA-17, 2 (Mar./Apr. 1981), 152–159.

[9] Nishikata, S., Muto, S. and Kataoka, T. (1982)
Dynamic performance analysis of self-controlled synchronous motor speed control systems.
IEEE Transactions on Industry Applications, IA-18, 3 (May/June 1982), 205–212.

[10] Reesor, D.B. (1984)
Control of a self-synchronous motor pump drive with a cycloconverter link.
M.S. thesis, University of Kentucky, 1984.